

# Optimal softening for force calculations in collisionless N-body simulations

E. Athanassoula<sup>1</sup>, E. Fady<sup>1</sup>, J.C. Lambert<sup>1</sup>, and A. Bosma<sup>1</sup>

<sup>1</sup> *Observatoire de Marseille, 2 Place Le Verrier, F-13248 Marseille Cedex 4, France*

Accepted . Received ;

## ABSTRACT

In N-body simulations the force calculated between particles representing a given mass distribution is usually softened, to diminish the effect of graininess. In this paper we study the effect of such a smoothing, with the aim of finding an optimal value of the softening parameter. As already shown by Merritt (1996), for too small a softening the estimates of the forces will be too noisy, while for too large a softening the force estimates are systematically misrepresented. In between there is an optimal softening, for which the forces in the configuration approach best the true forces. The value of this optimal softening depends both on the mass distribution and on the number of particles used to represent it. For higher number of particles the optimal softening is smaller. More concentrated mass distributions necessitate smaller softening, but the softened forces are never as good an approximation of the true forces as for not centrally concentrated configurations. We give good estimates of the optimal softening for homogeneous spheres, Plummer spheres, and Dehnen spheres. We also give a rough estimate of this quantity for other mass distributions, based on the harmonic mean distance to the  $k$ th neighbour ( $k = 1, \dots, 12$ ), the mean being taken over all particles in the configuration. Comparing homogeneous Ferrers ellipsoids of different shapes we show that the axial ratios do not influence the value of the optimal softening. Finally we compare two different types of softening, a spline softening (Hernquist & Katz 1989) and a generalisation of the standard Plummer softening to higher values of the exponent. We find that the spline softening fares roughly as well as the higher powers of the power-law softening and both give a better representation of the forces than the standard Plummer softening.

**Key words:** galaxies: structure – galaxies: kinematics and dynamics – methods: numerical.

## 1 INTRODUCTION

$N$ -body codes are often used to simulate the dynamical evolution of galaxies and galaxy systems, even though the number of particles that present day computer hardware and software can handle is smaller, by several orders of magnitude, than the number of stars in even a small galaxy. Because of this the particles do not represent individual stars, but should be considered as Monte-Carlo realisations of the mass distribution in a galaxy. In such simulations, when close encounters between individual particles are of no relevance to the physical problem under consideration, the gravitational force between two particles is smoothed, in order to reduce the spurious two-body relaxation due to a number of particles necessarily much smaller than the total number of stars in the system. Although a large softening

will ensure a low relaxation rate, we can not increase this value at will, since a high value of the softening introduces other drawbacks and in particular a bias to the gravitational force.

The question we will address in this paper is what value of the softening should be used in order for  $N$  particles to represent best a given density distribution. In a recent paper Merritt (1996, hereafter M96) argues that too small a value for the smoothing will give too noisy estimates, while too large a value will give a systematic misrepresentation of the force. M96 and Athanassoula *et al.* (1998; hereafter A+98) found that this optimal value of the softening depends on the number of particles  $N$  approximately as  $N^{-0.3}$ . In this paper we will extend previous work to other configurations, other  $N$ -body algorithms for calculating the force and other functional forms for the force approximation. The two  $N$ -

body methods under consideration are briefly described in section 2, where we present also the tools we will use for our comparisons. The optimal softening for the case of a Plummer sphere is discussed in section 3, including comparisons of *MISE* and *MASE*, as well as comparisons of calculations with GRAPE-3 and GRAPE-4. Section 4 presents the case of two Plummer spheres and section 5 two other density distributions, one more and the other less concentrated than the Plummer sphere. Section 6 discusses the effect of triaxiality, using the Ferrers' ellipsoid. Different types of softening are introduced in section 7 and a different way of calculating the force, using a hierarchical octal tree, in section 8. Finally our results are summarised and discussed in section 9.

## 2 METHODS

### 2.1 Force evaluation methods

Several methods have been developed for calculating the forces in self-consistent  $N$ -body simulations (see e.g. the reviews by Sellwood 1987 and Athanassoula 1993). They all have their advantages and disadvantages and which one should be chosen depends to a large extent on the problem to be solved. We will here briefly describe two methods not using either grids or expansions, in which case the introduction of the softening is more straightforward.

1) Direct summation. This method involves calculating the forces between every pair of particles and then summing up all contributions to the force on a given particle. It is straightforward, easy to program and easy to vectorise and parallelise. For a fixed number of particles it is by far the most accurate method, since its only approximation is the introduction of softening, and can be used without any restrictions on geometry. This method was used heavily in the seventies and early eighties, but was soon considered as a dead end because of its large claims in CPU time. Indeed the amount of time necessary for one force calculation scales as  $N(N-1)$ , where  $N$  the number of particles in the simulation. Thus, until recently, direct summation could not be used freely for simulations where a sufficiently high number of particles is necessary, as e.g. simulations of disc galaxies. Two major advances in computer hardware have changed the situation in the past few years.

The first is the advent of parallel machines, either SIMD or MIMD, which, given the simplicity of the communications involved in the direct summation method, make it possible to achieve relatively high performances with little software investment. A large number of such systems are actually in use, from the powerful many-node CRAY T3E, to "Beowulf" clusters, which have been recently implemented in many universities and research centers.

The second is the realisation of GRAPE, a dedicated computer card which performs the force calculation by direct summation and which can be coupled to a standard workstation allowing one to achieve at relatively low cost an excellent CPU performance. A series of such GRAPE boards have been built by the group in Tokyo University, starting with GRAPE-1 and evolving steadily to GRAPE-5, while new members of this family are under development. For a brief history of this project see Makino & Taiji (1998) and references therein. Boards with even numbers have high

accuracy arithmetic and can be used for collisional simulations, where close encounters play an important role in the evolution of the system, as for globular clusters and planetesimals. Boards with odd numbers have a more limited precision arithmetic and can only be used for collisionless systems. Thus GRAPE-3 uses 14 bits to represent the masses, 20 bits for the positions and 56 bits for the forces. Nevertheless this was shown to be sufficient for simulations (A+98), since the dominant source of error is the noise in the form of two-body relaxation, while the effect of the error in the force calculations is comparatively smaller (Hernquist *et al.* 1993, Makino 1994).

Two such systems have been used for the calculations presented in this paper, namely the GRAPE-3AF and GRAPE-4 systems in Marseille Observatory. The former consists of five GRAPE-3AF boards coupled via an Sbus/VMEbus converter to a Sun Ultra 2/200, and is described in detail in A+98. The latter consists of one GRAPE-4 processor board and one control board (Makino *et al.* 1997) linked to an Alpha 500/500 workstation via a PCI interface board (Kawai *et al.* 1997).

2) Treecodes. With the help of treecodes considerably more particles can be used in  $N$ -body simulations, while one of the main advantages of direct summation codes, namely that they can be applied to systems with any geometry, is preserved. They stem from the simple idea that when a group of particles is sufficiently distant from another particle and its spatial extent is small with respect to the distance separating it from the particle, then this group can be considered as one entity, and only monopole and, in some cases, quadrupole terms need be retained for the calculation of the force exerted by this group on the particle. Whether a group of particles can be considered as one entity, or whether it has to be further subdivided in subgroups is determined by the tolerance, or opening angle, which determines the precision of the force calculation. In this way one obtains a considerable saving over the number of force calculations necessary in a direct summation code, so that for tree-codes the necessary time increases with the number of particles  $N$  as  $N \log N$  or as  $N$ . The version of the treecode most commonly used in astronomy is the Barnes-Hut algorithm (1986) and in particular its vectorised version, freely available from Hernquist (1987).

The treecode shares several of the advantages of direct summation, namely that it can be applied to distributions with any geometry and large spatial and/or temporal density variations, while being considerably faster. It has, however, also many drawbacks. It is more difficult to program, and its vectorisation, and particularly parallelisation, present several difficulties. A more worrisome drawback is the fact that Newton's third law of motion is not necessarily obeyed. Take the example of an isolated particle A and a particle B in a cluster of particles far from A. Then the force of A on B is correctly calculated, while A will only feel the effect of the cluster of particles as a whole. Even so the *total* force on A from the whole of the cluster is adequately calculated and therefore one can expect a correct evolution of the system. Other drawbacks are discussed by Salmon and Warren (1994), who discussed the relative merits of opening angle criteria (or "Multipole Acceptability Criteria", as they call them).

The implementation of such a code on GRAPE systems

is possible, provided one keeps the monopole term only, and neglects quadrupole and higher order terms (Makino 1991, A+98). Such terms are nevertheless possible to include using a method described by Kawai & Makino (1999).

## 2.2 Notations and computing miscelanea

The usual way of softening the Newtonian force exerted on a particle by another particle is to by replace in the calculation of the potential the distance between the two particles,  $r$ , by  $\sqrt{r^2 + \epsilon^2}$ , where  $\epsilon$  is the softening parameter. In this way the acceleration (or force per unit mass) on particle  $i$  from  $N - 1$  other particles is written as:

$$\mathbf{F}_i = G \sum_{j=1}^N \frac{m_j (\mathbf{x}_j - \mathbf{x}_i)}{(|\mathbf{x}_i - \mathbf{x}_j|^2 + \epsilon^2)^{1.5}} \quad (1)$$

Here  $G$  is the gravitational constant which we hereafter take to be equal to unity. In the following we will assume for simplicity that all particles have the same mass, equal to  $m$ . Each term in eq. (1) is equal to the force felt by a point of unit mass in a Plummer sphere of scale-length  $\epsilon$ , and we shall thus hereafter refer to this softening for brevity as the Plummer softening. It was initially introduced by Aarseth (1963) in simulations of clusters of galaxies. Although this is the most commonly used form of the softened Newtonian force, it is not the only one. Alternative types of softening will be described in section 7.

Independent of the way softening is introduced, it is clear that too little smoothing leads to noise and too much of it to the modeling of a gravity which is far from Newtonian. In order to compare the calculated forces to the true ones M96 introduced the quantities *ISE* (Integrated Square Error), *ASE* (Average Square Error), *MISE* (Mean Integrated Square Error) and *MASE* (Mean Average Square Error). We will use them here also, since they provide a very useful way of quantifying how well the force of a given configuration is approximated. We will, however, modify them somewhat for our present needs, e.g. by introducing a multiplicative constant to make them dimensionless, so that it is possible to make comparisons between models with different total mass and size. We briefly summarise all the definitions below.

Let  $\mathbf{F}_{true}(\mathbf{x}_i)$  be the true force from a given mass distribution at a point  $\mathbf{x}_i$ , and let  $F_i$  be the force calculated at the same position from a given  $N$ -body realisation of the mass distribution and using a given softening and method. Then the average deviation between the two forces is given by

$$ASE = \frac{\mathcal{C}}{N} \sum_{i=1}^N |\mathbf{F}_i - \mathbf{F}_{true}(\mathbf{x}_i)|^2 \quad (2)$$

where the summation is over the  $N$  particles in the realisation. We can similarly introduce the “integrated square error”, or

$$ISE = \frac{\mathcal{C}}{M} \int \rho(\mathbf{x}) |\mathbf{F}(\mathbf{x}) - \mathbf{F}_{true}(\mathbf{x})|^2 d\mathbf{x} \quad (3)$$

where  $\rho(\mathbf{x})$  is the true density at point  $\mathbf{x}$ ,  $M$  is the total mass in the system,  $\mathbf{F}(\mathbf{x})$  is the force at position  $\mathbf{x}$  calculated from the  $N$ -body realisation of the mass distribution,

and the integral is taken over a volume in space encompassing the configuration. For spherically symmetric mass distributions using the *ISE* rather than the *ASE* brings a substantial gain in CPU time. Indeed the integration over the angles can be done analytically and one is left with a one-dimensional integration along a radius. We will sometimes refer to this as the radial *ISE* algorithm. For this the gain in time is proportional to  $n_{int}/(N-1)$ , where  $n_{int}$  is the number of points used when calculating the integral. Nevertheless this is made at the expense of considerable noise, since the number of points at which the integrand is calculated is relatively small. This will be discussed further in section 3.3.

In order to get rid of the dependence on the particular configuration, which is of no physical significance, we generate many realisations of the same smooth model and average our results over them. Thus the mean value of the *ASE* is

$$MASE = \frac{\mathcal{C}}{N} \langle \sum_{i=1}^N |\mathbf{F}_i - \mathbf{F}_{true}(\mathbf{x}_i)|^2 \rangle \quad (4)$$

where  $\langle \rangle$  indicates an average over many realisations. Similarly for the mean value of the *ISE* we get

$$MISE = \frac{\mathcal{C}}{M} \langle \int \rho(\mathbf{x}) |\mathbf{F}(\mathbf{x}) - \mathbf{F}_{true}(\mathbf{x})|^2 d\mathbf{x} \rangle \quad (5)$$

Values of  $\epsilon$  minimising the *MISE* or the *MASE* should give the optimal representation of the force of the system.

In the above  $\mathcal{C}$  is a multiplicative constant, introduced to permit comparisons between different mass distributions. If we only want to assess the effect of the number of particles, as in M96 and sections 3 and 6, we can simply use  $\mathcal{C} = 1$ . On the other hand if more than one configuration are to be compared then it may be necessary to use the multiplicative constant  $\mathcal{C}$ . To make this clearer let us consider two Plummer spheres of the same mass, and of which the second one has double the scale length of the first one. In that case the optimal softening for the second should be double the optimal softening for the first one. By rescaling the second Plummer sphere, i.e. multiplying all distances by 0.5, we would get for both the same softening, which is obvious since they are in fact the same object. It is thus preferable to compare softenings after the objects have been rescaled to the same mass and size. In a similar way if we want to compare the appropriate softening for a Plummer sphere and that of a Dehnen sphere we first have to rescale one of the two so that the two objects correspond to the same mass and size, otherwise the comparison would not be meaningful, and would only tell us that bigger objects need bigger softenings. Once the objects are rescaled to the same mass and size, then the comparison of the optimal softenings could tell us something about the effect of the central concentration. Such a rescaling is, however, not possible in all cases. If in a simulation we want to see e.g. the evolution of a given Plummer sphere in presence of a given Dehnen sphere, then we can not rescale each component separately, without changing the problem we are considering. In this case we have to search for the softening that would help best represent the entire configuration, and then compare it with the softening that represents best each of the two unscaled objects individually. The above is of course only common sense. We have nevertheless explained it in some

detail here since otherwise it may be unclear to the reader why, in the following sections, in some cases we use a scaling and in others we do not.

We will use the following definition for  $\mathcal{C}$  which makes the *MISE* and *MASE* quantities dimensionless:

$$\mathcal{C} = F^{-2}(\mathcal{R})$$

or, equivalently,

$$\mathcal{C} = \mathcal{R}^4 M^{-2}$$

Here  $M$  is the total mass in the configuration,  $\mathcal{R}$  is a characteristic radius, e.g. the half mass radius, and  $F(\mathcal{R})$  is the force at that radius. Similarly, in such cases, the softening should also be scaled with the adopted characteristic radius, since it has units of length.

It is debatable whether in the definition of *ISE* it would have been better to use the numerical or the analytical density of the configuration. We have chosen the latter for two reasons. One is continuity with the definition of M96, and the other is that the calculation of the density of an  $N$ -body configuration is not straightforward and may, by itself, introduce further uncertainties and complications. As will be shown in the next section, for sufficiently large number of realisations, the present definitions of *MISE* and *MASE* give the same results and this legitimises our choice for the density.

In all the examples in this paper, unless otherwise stated, we have used  $6 \times 10^6/N$  realisations. Because of the high CPU speed of our two GRAPE systems we have used, whenever possible, *MASE* calculations on GRAPE. The two notable exceptions are the calculations with alternative softening (section 7) and the calculations with the standard treecode (section 8), both of which can not be done on GRAPE, and for which we have confined ourselves to radial *MISE* calculations.

For the treecode calculations on GRAPE we have used the software described in detail in A+98. For the standard treecode calculated on a workstation we have used the Barnes version of the Barnes-Hut algorithm (Barnes and Hut 1986) included in the NEMO package (cf. Teuben 1995). This version of the treecode can use up to quadrupole terms.

For the integration along the radius in the radial *ISE* calculation we use the alternative extended Simpson's rule (Press *et al.* 1988), which has an accuracy of  $\mathcal{O}(N^{-4})$ , and 100 points along the line of integration. For the calculation of the radial *ISE* values for the Plummer sphere we have used as an upper limit of the integration  $L = 20a_p$ , where  $a_p$  is the scale-length of the Plummer sphere. This radius contains more than 99% of the mass of the Plummer model, while the density has fallen to roughly  $3 \times 10^{-7}$  of its central value.

### 3 OPTIMAL SMOOTHING FOR A PLUMMER SPHERE DENSITY DISTRIBUTION

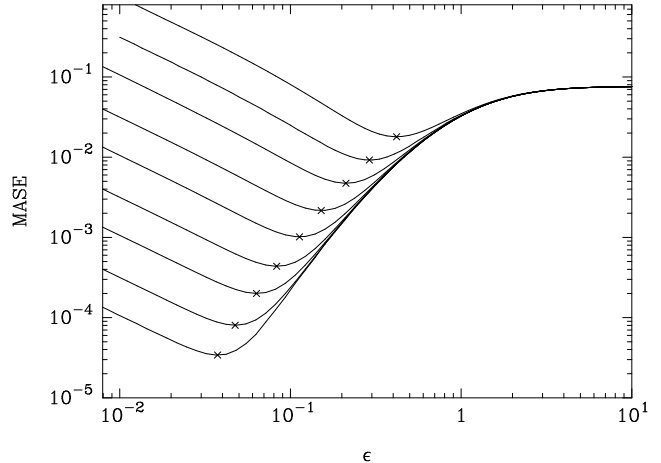


**Figure 1.** *MASE* as a function of the softening  $\epsilon$  for a Plummer sphere. From top to bottom the curves correspond to  $N = 30, 100, 300, 1\,000, 3\,000, 10\,000, 30\,000, 100\,000, 300\,000$ , where  $N$  is the number of particles in the realisation of a Plummer sphere. The number of realisations taken for the mean is  $6 \times 10^6/N$ . The position of the minimum error along a line corresponding to a given  $N$  is marked by an  $\times$ , and the corresponding  $\epsilon$  value is the optimal softening  $\epsilon_{opt}$  for this number of particles.

#### 3.1 Dependence of the error on the softening and the number of particles

Following M96 and A+98 we will use, as a first model, a truncated Plummer sphere

$$\rho(r) = \begin{cases} \frac{3M_T}{4\pi a_p^3} (1 + r^2/a_p^2)^{-5/2} & r \leq R \\ 0 & r > R \end{cases}$$

where  $M_T$  is the mass of the Plummer sphere had it extended to infinity,  $a_p$  is its scale-length and  $R$  is its truncation radius. For the remainder of this paper, unless otherwise noted, we will adopt, without loss of generality,  $a_p = 1$ , as a truncation radius the radius containing 0.999  $M_T$ , and the mass within the truncation radius,  $M(\leq R) = 1$ . The corresponding radial *MISE* and *MASE* values were calculated in M96, for  $N$  between 30 and 30 000, and in A+98 for  $N$  between 30 and 300 000 with direct summation and 1 000 000 using a tree code. It was found that, as expected, the error for a given number of particles  $N$ , be it radial *MISE* or *MASE*, shows a minimum for a given value of  $\epsilon$ . In Figure 1 we show a number of examples for various values of  $N$ . The information is essentially the same as in Figure 4 of A+98, except now for *MASE* rather than radial *MISE*.

For small values of the softening the noise dominates the error. For this reason the *MASE*, for such values of the softening, decreases steeply with  $N$ , the number of particles in the configuration. Conversely for large values of the softening it is the bias that dominates. For a sufficiently large value of the softening the *MASE* does not show any dependence, either on the softening, or on the number of particles. In this region the inter-particle forces go as  $r\epsilon^{-3}$ , and tend to zero as  $\epsilon \rightarrow \infty$ . Thus, for sufficiently large values of the softening, the  $\mathbf{F}_{true}(\mathbf{x})$  term dominates in the difference in equations (2), (3), (4) and (5) and *MISE* and *MASE* tend to

$$\left\langle \int \rho(\mathbf{x}) |\mathbf{F}_{true}(\mathbf{x})|^2 d\mathbf{x} \right\rangle \quad (6)$$

and

$$\left\langle \frac{1}{N} \sum_{i=1}^N |\mathbf{F}_{true}(\mathbf{x}_i)|^2 \right\rangle \quad (7)$$

respectively. These quantities depend only on the mass distribution in the configuration, and are independent of both the softening and the number of particles, as borne out in Figure 1.

In between the region dominated by the noise and that dominated by the bias there is a minimum of the error. Since the noise decreases considerably with  $N$ , while the bias is not affected by it, the minimum error should decrease with increasing  $N$  and should move to smaller values of the softening, as is indeed shown to be the case in Figure 1.

### 3.2 The optimal value of the softening and the corresponding value of the error

Let us call  $\epsilon_{opt}$  the value of  $\epsilon$  which gives the best representation of the force, i.e. gives the lowest value of  $MISE$  or  $MASE$  (which we will denote hereafter by  $MISE_{opt}$  or  $MASE_{opt}$ ). Using least square fits, M96 showed that power laws give good fits for the values of  $\epsilon_{opt}$  and  $MISE_{opt}$  as a function of  $N$ , the number of particles in the configuration. For  $N$  between 30 and 300 000, and  $\mathcal{C} = 1$ , A+98 obtained

$$\epsilon_{opt} = 0.98N^{-0.26}$$

and

$$MISE_{opt} = 0.22N^{-0.68}$$

When few particles are used (M96) the exponent of the  $N$  dependence of  $\epsilon_{opt}$  takes a value around -0.28 and that of  $MISE_{opt}$  around -0.66. If we consider  $N$  values between 10 000 and 300 000 then these values change to -0.23 and -0.76, while the asymptotic values for  $N \rightarrow \infty$  are -0.2 and -0.8 (A+98). This argues that the above equations are only approximate and that in fact the exponents are functions of the number of particles considered. Nevertheless, within the range of particle numbers used in most collisionless  $N$ -body simulations they constitute a very good approximation.

### 3.3 Comparing $MISE$ and $MASE$

$ISE$  and  $ASE$  are, of course, only different ways of calculating the same integral. In the case of radial  $ISE$ , however, the hypothesis is implicitly made that the configuration is spherically symmetric, which is obviously true for the continuum distribution, or in the limit of an infinite number of particles, but not, strictly speaking, in the case of a representation of a Plummer sphere with a finite number of particles. A different way of seeing the same effect is to say that many more points are used in the sampling of the forces in case of an  $ASE$  than in the case of this  $ISE$ . Thus the  $ASE$  ( $MASE$ ) errors are smaller than the corresponding radial  $ISE$  ( $MISE$ ) ones for the range of values of  $\epsilon$  considered e.g. in Figure 1, except for the largest values ( $\epsilon$  greater than

or of the order of 1.5), where the bias predominates and the contribution from the noise is very small. This advantage is linked to a corresponding disadvantage, namely that the CPU time necessary for calculating an  $ASE$  is larger than the corresponding time for an  $ISE$  calculation by a factor  $(N-1)/n_{int}$ , where  $N$  the number of particles in the representation and  $n_{int}$  the number of points at which the integrand is calculated. This makes the  $MASE$  calculations prohibitively expensive, even on powerful workstations. On the other hand GRAPE-3 and GRAPE-4 are well adapted for such calculations. Thus a  $MASE$  calculation for 100 000 particles goes roughly 2000 times faster on our GRAPE-3AF system than on its front end, an Ultra 2/200.

### 3.4 Comparing results with GRAPE-3 and GRAPE-4

Comparing the  $MASE$  results calculated with GRAPE-3 and GRAPE-4, respectively, we find that they agree very well. This could, at first sight, seem at odds with the fact that GRAPE-3 has a much more limited accuracy than GRAPE-4 that has near 64-bit precision. As argued, however, in A+98, the error in GRAPE-3 comes from round-off and can therefore be considered as random. Thus when one adds the forces from many particles this error cancels out and one obtains an accuracy similar to what is obtained on GRAPE-4. For this reason we have used both GRAPE systems for the calculations given in the next few sections.

## 4 THE CASE OF TWO PLUMMER SPHERES

In most simulations of galaxies or systems of galaxies it is necessary to represent more than one component, each having considerably different properties. In order to assess the effect of this on the choice of the softening we will in this section consider the case of two non-truncated Plummer spheres. The first one has a scale-length  $a_1 = 1$  and the second one a scale-length  $a_2 = 0.1$ . We consider mass ratios of the two components  $M_1/(M_1 + M_2) = 0, 0.1, 0.25, 0.5, 0.75, 0.9$  and 1. The total mass is in all cases equal to 1, the total number of particles equal to 100 000 and the total number of realisations equal to 40. We also consider two spatial configurations, one in which the two spheres are concentric and the other in which their centers are at a distance of 10 length units. For some mass ratios the former configuration can be considered as representing crudely a halo and bulge system, and the latter a halo of a target galaxy with a spherical companion. We will discuss further only the case of the two concentric spheres, since the two configurations give essentially the same results for  $MASE$ . As will be later shown in the next section it is the distance to the nearest neighbours that mainly determines  $MASE$  and the corresponding  $\epsilon_{opt}$ , and this depends essentially on the density of the Plummer sphere with the smallest scale-length, rather than on its location.

Let us first discuss the case of a single simulation in which more than one component is present. Since in this case we can not apply a separate scaling to each component (cf. section 2) we have to take  $\mathcal{C} = 1$ . Fig 2 compares the  $MASE$  curves for the seven mass ratios under consideration, and shows that more concentrated configurations have

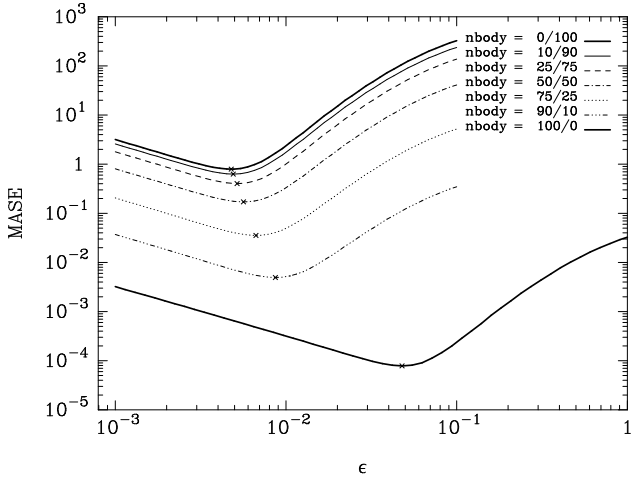


**Figure 2.** *MASE* as a function of  $\epsilon$  for 100 000 particle configurations. The lower heavy line corresponds to a Plummer sphere of unit scale-length and the upper one to a Plummer sphere of 0.1 scale-length. The remaining ones correspond to cases where both Plummer spheres are present, with mass ratios as given in the figure. The  $\times$  symbols show the positions of the minimum on each curve. As discussed in the text, for these plots we have used  $\mathcal{C} = 1$ , since we are considering all components present in the same simulation.

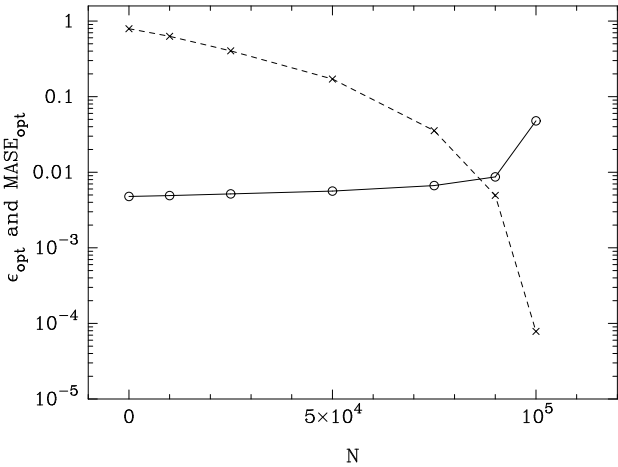


**Figure 3.** Optimal softening (open circles) and corresponding  $MASE_{opt}$  ( $\times$ ) as a function of the number of particles in the least dense component. The points represented here are obtained from calculating the minima of the curves of the previous figure.

larger errors and smaller corresponding  $\epsilon_{opt}$  than less concentrated ones. The difference between the respective curves is considerable, since a change of a factor of 10 in the scale-length makes a change of more than  $10^4$  in  $MASE_{opt}$  and of roughly 10 in  $\epsilon_{opt}$ . This figure also shows that in an  $N$ -body simulation with many components the force on the densest components will be less well represented than the force on

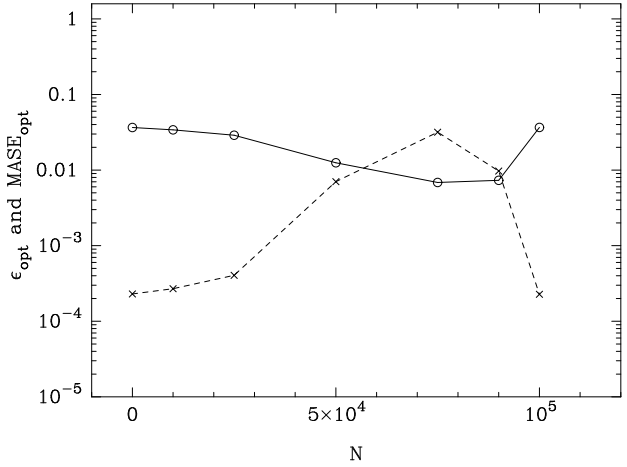


**Figure 4.** Optimal softening (open circles) and corresponding value of the *MASE* ( $\times$ ) as a function of the number of particles in the least dense component.

the more extended ones. The total error is bigger when the percentage of mass in the denser component is larger. We also note that the increase in the error obtained by substituting 10% of the particles in a loose configuration with a denser one is very big, whereas the decrease in the error obtained by substituting 10% of the particles in a dense configuration by a looser one is quite small. This is further stressed in Figure 3, which is obtained from the minima of the curves in Figure 2, and shows how the optimal softening depends on the percentage of mass in the least dense component. Similar calculations (not illustrated here) show that there is hardly any difference between the cases where the two Plummer spheres are concentric and the case where they are separated, which leads to the conclusion that the densest part influences the result always in the same way, independent of its location in the configuration.

Now let us consider a different question and compare seven different simulations, in each of which one of the above seven configurations is present. Since now the scaling can be applied independently to each of the configurations, in order to compare these cases between them we need to use the weighted versions of the *MASE* definition and softening. Since the total mass of all the configurations is the same, the only factor that is changing from one configuration to another is the half mass radius, which takes respectively the values 0.13, 0.14, 0.18, 0.45, 0.97, 1.18 and 1.30. Now the result of the least dense ( $a_P = 1$ ) and most dense ( $a_P = 0.1$ ) configuration are of course identical. This simply reflects the fact that the densest Plummer sphere can be represented as well as the least dense one, provided one uses appropriately weighted softening values. This is clear also from Figure 4 which shows  $MASE_{opt}$  and  $\epsilon_{opt}$  as a function of the percentage of mass in the least dense component. This figure also shows that, from the configurations analysed here, the largest error corresponds to the case with 25% of the particles in the more concentrated Plummer sphere. This is also the configuration for which  $\epsilon_{opt}$  is minimum.

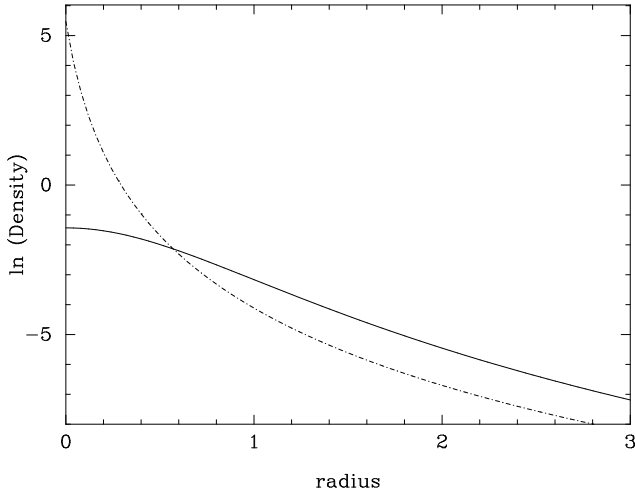


**Figure 5.** Comparing the density distributions of the Plummer sphere (solid line) and the Dehnen  $\gamma = 0$  sphere (dot-dashed line) used in section 5.

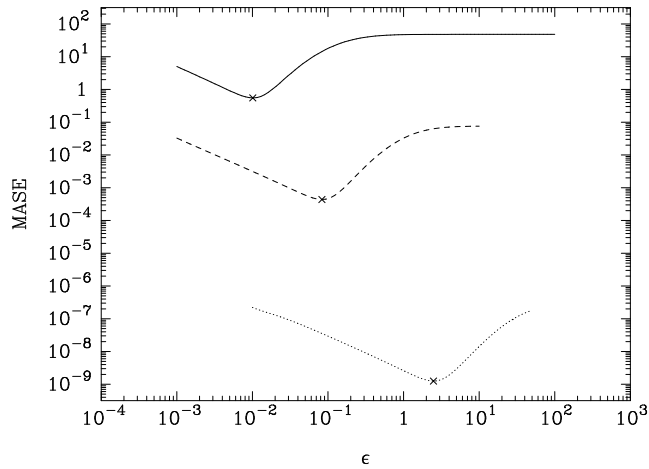


**Figure 6.** Comparing the unweighted *MASE* as a function of  $\epsilon$  for six hundred 10 000 particle representations of a truncated homogeneous sphere (dotted line), a Plummer sphere (dashed line) and a Dehnen sphere of index  $\gamma = 0$  (solid line).

## 5 THE EFFECT OF CENTRAL CONCENTRATION

### 5.1 Comparison of three different spherical distributions

We have so far considered the case of a Plummer sphere, a mass distribution frequently used in astrophysics. In this section we will consider two other density distributions, a truncated homogeneous sphere and a Dehnen sphere (Dehnen 1993). The former is less centrally concentrated than the Plummer sphere and the latter more, so that by comparing the respective *MISE* or *MASE* we can test the effect of central concentration on the optimal  $\epsilon$  and on the

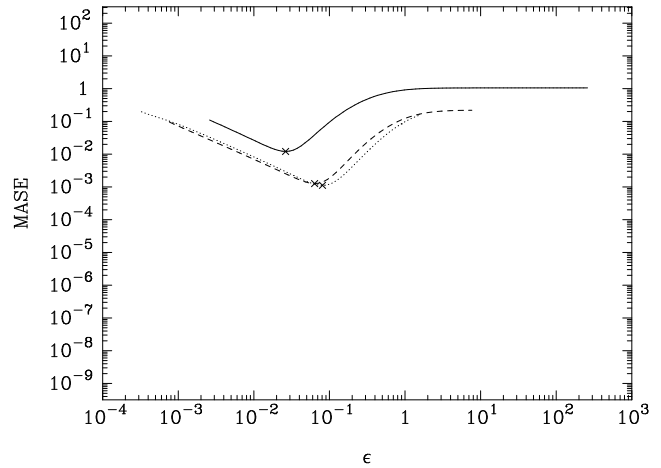


**Figure 7.** Comparing the weighted *MASE* as a function of  $\epsilon$  for six hundred 10 000 particle representations of a truncated homogeneous sphere (dotted line), a Plummer sphere (dashed line) and a Dehnen sphere of index  $\gamma = 0$  (solid line).

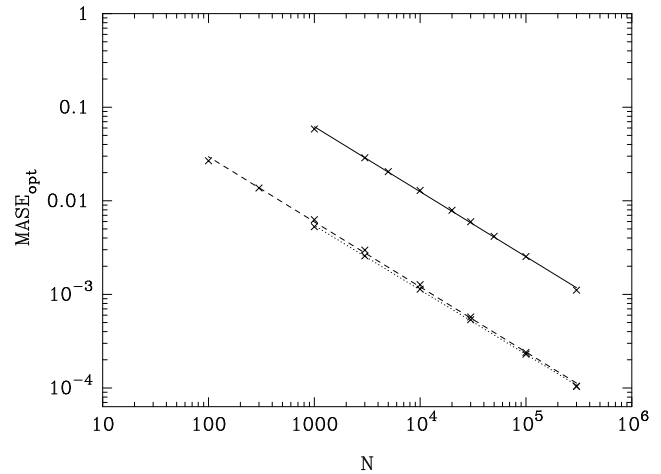


**Figure 8.**  $MASE_{opt}$  as a function of  $N$  for a truncated homogeneous sphere (dotted line), a truncated Plummer sphere (dashed line) and a truncated Dehnen sphere of index  $\gamma = 0$  (solid line).

corresponding accuracy. Since both Plummer and Dehnen spheres extend to infinity, we have introduced in both cases a cut-off radius, taken so that the mass within that radius is equal to 0.999 times the total mass.

The density profile of the homogeneous sphere is

$$\rho(r) = \begin{cases} 3M_T/4\pi R^3 & r \leq R \\ 0 & r > R \end{cases}$$

where  $R$  is its outer radius and  $M_T$  its total mass. For the Dehnen sphere we have

$$\rho(r) = \begin{cases} \frac{(3-\gamma)M_T}{4\pi} \frac{a_D}{r^\gamma (r+a_D)^{(4-\gamma)}} & r \leq R \\ 0 & r > R \end{cases}$$

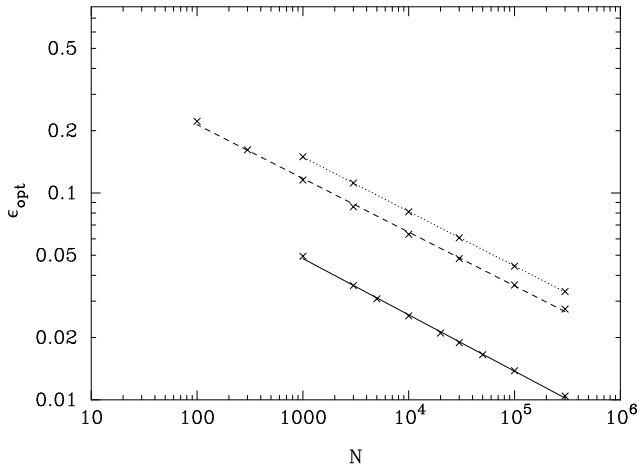


**Figure 9.**  $\epsilon_{opt}$  as a function of  $N$  for a truncated homogeneous sphere (dotted line), a truncated Plummer sphere (dashed line) and a truncated Dehnen sphere of index  $\gamma = 0$  (solid line).

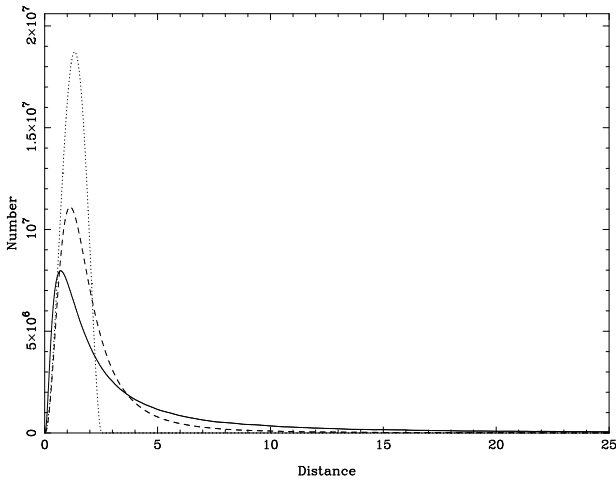


**Figure 10.** Histogram for inter-particle distances for the homogeneous sphere (dotted line), the Plummer sphere (dashed line) and the Dehnen  $\gamma = 0$  sphere (solid line).

where  $M_T$  is its total mass,  $a_D$  is its scale-length and  $\gamma$  is its concentration index, determining the slope of the density at the origin. For the examples discussed below we took  $a_D = 0.1$  and  $\gamma = 0$ .

The truncation radii, containing 0.999 of the total mass, are equal to 299.8 and 38.71 for the Dehnen and Plummer configuration respectively. For the homogeneous sphere we have also taken  $R = 38.71$  and in all three models we have taken the mass within the truncation radius to be equal to 1. The Plummer and Dehnen density distributions are compared in Figure 5.

Figure 6 and 7 compare the results for  $MASE$  obtained from six hundred representations of 10 000 particles each. In the former we use the un-weighted definition of  $MASE$

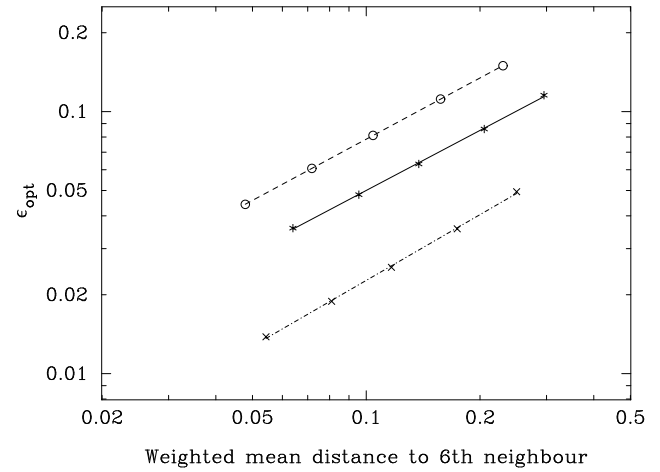


**Figure 11.** Optimal softening as a function of mean distance to the 6th nearest neighbour. Values for the homogeneous sphere are given by open circles and a dashed line, values for the Plummer sphere by asterisks and a full line and values the Dehnen sphere by  $\times$  symbols and a dot-dashed line.

(i.e. with  $C = 1$ ) and of the softening, and in the latter the weighted definition. We note that, in both cases, the Dehnen sphere, which is the most concentrated of the three configurations, requires smaller softening values and is always less accurately represented than the two more spread out configurations, in good agreement with the results of section 4. The differences, however, are much more important in the comparison of the un-weighted  $MASE$ . Furthermore in this case the differences between the Plummer and the homogeneous sphere are very large, while when the comparison is between the weighted functions the difference is very small. Again this is in agreement with the results of section 4. If we simulate all three spheres in the same configuration we have to use for all cases the same softening and  $C = 1$ . Now the forces of the Dehnen sphere will be very badly represented and those of the homogeneous sphere very well. The situation is totally different if we are simulating one of those spheres only, because then we have to calibrate the lengths appropriately, so that all systems have the same half-mass radius. Now the Dehnen sphere will do much better than in the un-weighted case, and the homogeneous sphere much worse. Thus the weighted  $MASE_{opt}$  is respectively 0.001, 0.001 and 0.01 for the homogeneous, Plummer and Dehnen spheres. In particular the differences between the Plummer and the homogeneous sphere are very small. The  $MASE_{opt}$  for the Dehnen sphere is considerably larger than for the other two, presumably because, in the Dehnen sphere, we are trying with a single value of the softening to accommodate both very dense and very sparse regions.

Figures 8 and 9 compare weighted  $MASE_{opt}$  and  $\epsilon_{opt}$  as a function of  $N$  for the three configurations and confirm the trend seen in Figure 7. The dependence of  $MASE_{opt}$  and  $\epsilon_{opt}$  on  $N$  for all three density distributions can be represented by power laws

$$MASE_{opt} = BN^b \quad (8)$$



**Table 1.** Coefficients of the power laws in equations 8 and 9

Mass distribution	A	a	B	b
Homogeneous sphere (un-weighted)	28.	-0.26	$7.1 \times 10^{-7}$	-0.69
Plummer sphere (un-weighted)	0.84	-0.25	0.32	-0.72
Dehnen $\gamma = 0$ sphere (un-weighted)	0.12	-0.27	340.	-0.69
Homogeneous sphere (weighted)	0.92	-0.26	0.63	-0.69
Plummer sphere (weighted)	0.64	-0.25	0.94	-0.72
Dehnen $\gamma = 0$ sphere (weighted)	0.32	-0.27	7.5	-0.69

and

$$\epsilon_{opt} = AN^a \quad (9)$$

The values of the coefficients are given in Table 1. Since the exponent in the above dependences depends somewhat on the range of  $N$  used (cf. A+98 and section 3.2), we used for the three mass distributions the same values of  $N$  for the linear fits, namely the values for  $N = 1\,000$ ,  $3\,000$ ,  $10\,000$ ,  $30\,000$ ,  $100\,000$  and  $300\,000$ .

The table and figures show clearly that more centrally concentrated configurations need smaller values of the softening for an optimal representation of the force, and the precision achieved is never as good as for less centrally concentrated configurations. The minimum error,  $MASE_{opt}$ , decreases somewhat faster with  $N$  for the case of the Plummer sphere, but the differences are small.

Figure 10 compares the histograms of the inter-particle distances for the three models after they have been rescaled so that the half-mass radii are in all three cases the same. This scaling is appropriate for understanding the results obtained with weights. Each histogram has been obtained from ten 10 000 particle realisations of each model. We note that the peak of the histogram is nearest to the center for the Dehnen sphere, followed by the Plummer sphere, while the peak of the histogram for the homogeneous sphere is yet further out. It is thus expected that there are more particles very close to each other in the Dehnen sphere than in the Plummer one, and even more compared to the homogeneous one. However the Dehnen sphere has also more particles with very large inter-particle distances, while these are fewer for the Plummer sphere and even more so for the homogeneous sphere.

## 5.2 Extension to other configurations

The results shown in Figure 9 give us the optimal value of the softening, which gives the best representation of the forces, as a function of the number of particles  $N$ . However they also show that a value of softening which is optimal for one type of mass distribution is not necessarily optimal for another, and that the optimal value depends strongly on the central concentration of the distribution. Thus, in order to find  $\epsilon_{opt}$  for a mass distribution other than the three discussed here, one can either do the full calculations of the  $MASE$ , as above, or use the above results to obtain rough estimates. Since the former is rather demanding, we would like, in the remaining of this section, to see whether it is

possible to obtain some, albeit crude, estimates of the optimal softening as a function of quantities linked to the mass distribution, but more straightforward to calculate than the  $MASE$ .

As we have already seen, smaller values of the softening are necessary for more compact configurations or for representations with a larger number of particles, i.e. in cases where the particles are closer together. This suggests that some measure of inter-particle distances could be used for estimating the optimal value of the softening. Furthermore, since  $MASE$  is more dependent on the accuracy of the forces to nearby particles, we will try using the distances of the few nearest neighbours. Let us thus, for a given configuration, measure, for every particle, the distance to its twelve nearest neighbours. Now we need to average this over all particles in the configuration, in order to obtain, for the whole configuration, the mean distance to the nearest neighbour, the mean distance to the second nearest neighbour etc., up to the mean distance to the 12th nearest neighbour. A standard arithmetic average would not be appropriate for this. This can be understood if we mentally add to the configuration a single particle, located so far from it that it can, for argument's sake, be considered at infinity. This new particle will not influence the value of  $MASE$ , the value of  $\epsilon_{opt}$  that should be used, or the accuracy in the force calculations. On the other hand it will influence the mean distance to the  $k$ th neighbour. It is thus not reasonable to expect a close relation between  $\epsilon_{opt}$  and the arithmetic mean of the  $k$ th closest neighbour of all particles. For this reason, instead of the standard arithmetic mean, we will prefer using the harmonic mean

$$r_{k,mean1} = (N^{-1} \sum_{i=1}^N r_{k,i}^{-1})^{-1}$$

or, since the force is inversely proportional to the square of the distance,

$$r_{k,mean2} = (N^{-1} \sum_{i=1}^N r_{k,i}^{-2})^{-1/2}$$

where the summations are over all the particles in the configuration and  $k = (1, \dots, 12)$ . In this way we obtain for a given configuration the mean distance to the nearest neighbour, the mean distance to the second nearest neighbour etc., up to the mean distance to the 12th nearest neighbour. It is possible to diminish the noise in such calculations by considering several realisations of the same configuration and then mean  $r_{k,mean1}$  or  $r_{k,mean2}$ , now using simple arithmetic means over all realisations. We calculated these mean inter-particle distances as a function of  $N$  for the three density distributions considered above, using  $3 \times 10^6/N$  realisations. In all cases the dependence is roughly linear on a log-log plane, and thus can be represented by power laws of the type

$$r_{k,mean} = AN^a$$

where  $r_{k,mean}$  is equal to  $r_{k,mean1}$  or  $r_{k,mean2}$ . In both cases the value of  $a$  is around -0.33 or -0.34 and does not depend

**Table 2.** Coefficients of the power laws in equation (10)

Neighbour	Homogeneous		Plummer		Dehnen	
	A	a	A	a	A	a
1	0.95	0.78	0.55	0.76	0.31	0.83
3	0.59	0.78	0.35	0.76	0.19	0.83
5	0.50	0.78	0.30	0.76	0.16	0.83
7	0.45	0.78	0.28	0.76	0.15	0.83
9	0.41	0.77	0.26	0.76	0.14	0.84
11	0.39	0.77	0.25	0.76	0.13	0.84

much on which of the twelve nearest neighbours is considered. The latter is not true if we use standard means. The values of A depend of course on which of the nearest neighbours is chosen.

We have thus obtained so far, for a given density distribution and a given number of particles  $N$ , the average distance to the  $k$ th nearest neighbour, for  $k$  between 1 and 12, as well as an optimal softening  $\epsilon_{opt}$  (cf. Figure 9). From these two we can eliminate the dependence on  $N$  and obtain the dependence of  $\epsilon_{opt}$  directly on the average distance to the  $k$ th nearest neighbour. This is given in Figure 11 for the sixth neighbour, after both distances and the softening have been weighted appropriately, as discussed in section 2. We have repeated this exercise for all other values of  $k$  between 1 and 12, but since the results are similar we do not reproduce them here. Again a power law gives a good representation of the dependences

$$\epsilon_{opt} = Ar_{k,mean}^a \quad (10)$$

The values of A and a, for various neighbours are given in Table 2.

Figure 11 can give some, albeit rough, estimate of the optimal softening to be used, once an  $r_{k,mean}$  has been calculated, since the differences between the three models are less, or of the order of, 0.5 dex. It is, however, possible to narrow down the prediction further. Indeed the three dependences are ordered as a function of the central concentration of the corresponding models, less concentrated models corresponding to higher softening than more concentrated ones, in good agreement with what was previously discussed in this section. Thus comparing the central concentration of the new model, whose optimal softening we want to estimate, with that of the three considered here, should probably narrow the estimate to 0.2 or 0.3 dex.

## 6 THE EFFECT OF TRIAXIALITY

So far we have considered only spherical objects. By using, however, the *MASE* rather than the radial *MISE* accuracy estimator it is possible to consider non-spherical configurations. As an example we will in this section consider a Ferrers' ellipsoid (Ferrers 1877), a distribution often used for modeling bars. The corresponding density is

$$\rho = \begin{cases} \rho_0(1 - g^2)^n & \text{if } g < 1 \\ 0 & \text{otherwise} \end{cases}$$

where  $g^2 = x^2/a^2 + y^2/b^2 + z^2/c^2$ ,  $a > b > c$  are the major, intermediate and minor axes,  $\rho_0$  is the central density of the ellipsoid and  $n$  is an index determining the mass distribution in the ellipsoid. We calculated *MASE* values for four such

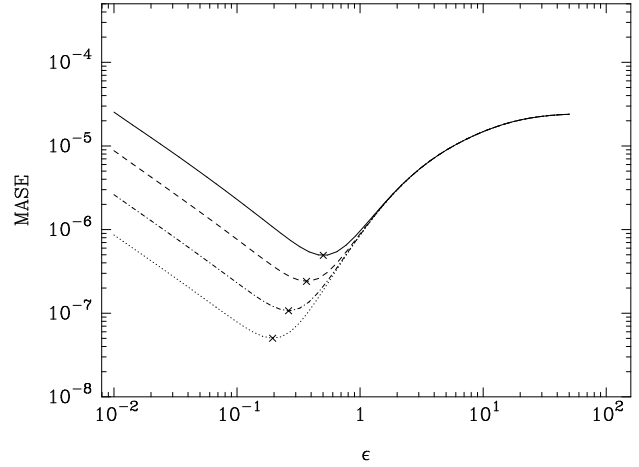


**Figure 12.** *MASE* as a function of softening for a homogeneous Ferrers ellipsoid of axial ratio 10:10:1. The various curves correspond to a different number  $N$  of particles in the configuration; 10 000 (solid line), 30 000 (dashed line), 100 000 (dot-dashed line), and 300 000 (dotted line), respectively.

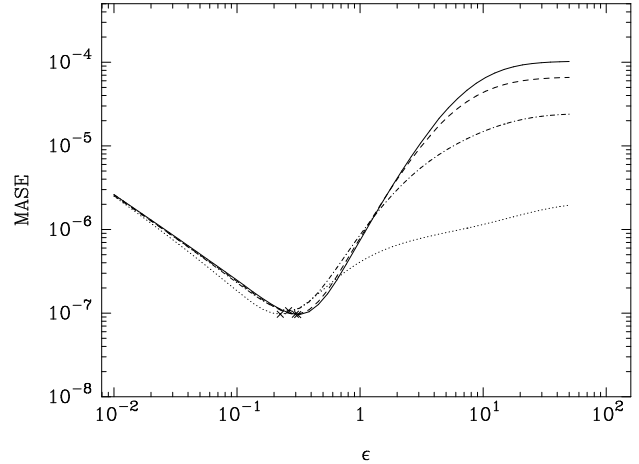


**Figure 13.** *MASE* as a function of softening for four Ferrers' ellipsoids of axial ratio 1:1:1 (solid line), 12:4:3 (dashed line), 10:10:1 (dash-dotted line) and 74:74:1 (dotted line). In all cases the number of particles is equal to 100 000 and the number of realisations is equal to 60.

ellipsoids with  $n = 0$  and  $a : b : c = 1:1:1$ , 12:4:3, 10:10:1 and 74:74:1 respectively. These represent objects common in an astrophysical context: a sphere, a bar, a thin and a very thin disc. Undoubtedly the disc component in real galaxies is not as thin as the thinnest of the two discs that we are using here, but we have added on purpose this rather extreme ellipsoid to see how an extreme thinness would affect the values of *MASE*. To facilitate comparisons, the four ellipsoids have been taken to have the same volume and mass (equal to 666.666 and 1 respectively), so we can take  $\mathcal{C} = 1$ .

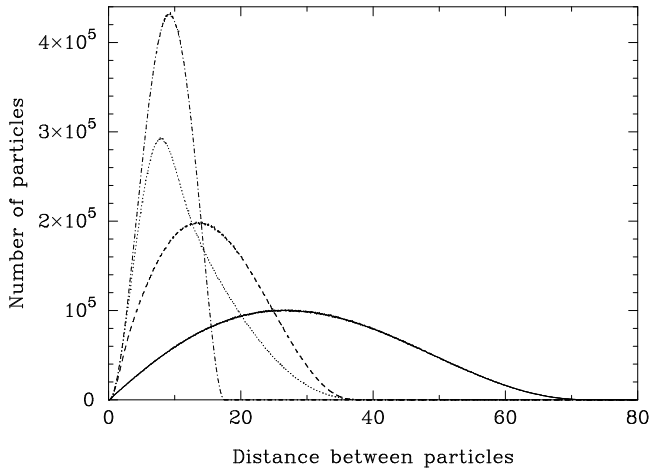


**Figure 14.** Histogram of inter-particle distances of all pairs of particles in Ferrers' homogeneous ellipsoids with axial ratio 1:1:1 (dot-dashed line), 12:4:3 (dotted line), 10:10:1 (dashed line) and 74:74:1 (solid line). Each histogram was obtained from ten 10 000 particle realisations.

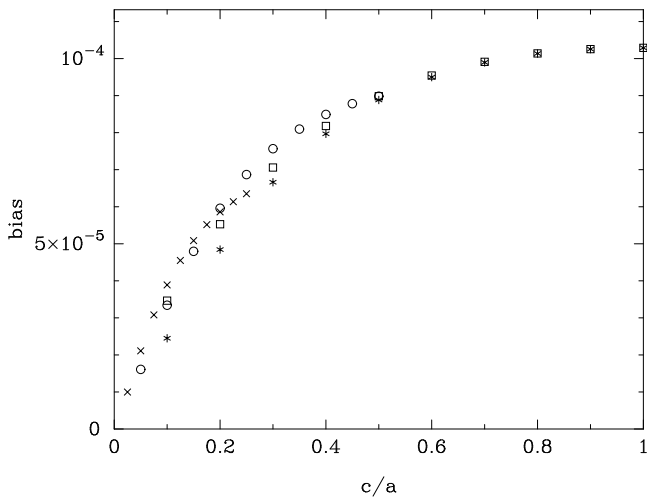


**Figure 15.** Bias for a softening tending to infinity as a function of the axial ratio  $c/a$  of the ellipsoid. Asterisks correspond to oblate ellipsoids and open squares to prolate ones. Open circles and  $\times$  correspond to axial ratios  $a : a/2 : c$  and  $a : a/4 : c$  respectively. All ellipsoids have the same volume as the four studied in more detail in this section.

Figure 12 shows  $MASE$  as a function of the softening for a Ferrers homogeneous ellipsoid of axial ratio 10:10:1 and different values of  $N$ . The general outline of the curves is the same as for the spherical objects (cf. section 3.1). As is the case for the spherical distributions  $\epsilon_{opt}$  can be represented by a power law dependence on the number of particles  $N$ .

In order to evaluate better the effect of triaxiality on the error in the force calculation we plot in Figure 13 the  $MASE$  as a function of  $\epsilon$  for the four ellipsoids under con-

sideration. In order not to burden the figure we plot only one value of  $N$ , in this case 100 000. Similar results have been obtained for the other values of  $N$  considered. Let us first consider the flat part of the curve, where the  $MASE$  is practically independent of the softening, and which occurs for large values of  $\epsilon$ . For brevity we will hereafter call this the bias part of the curve. Two effects in particular are clear from Figure 13 about the bias part. The first concerns for how big a value of the softening this part is attained and the second what the value of  $MASE$  on this section is.

Figure 13 shows that the bias part occurs for relatively smaller  $\epsilon$  values when the shape is spherical, and considerably larger ones when the departure from sphericity is large. This can be understood with the help of Figure 14, which compares histograms of the inter-particle distances for the four ellipsoids under consideration. We note that, as expected, the higher the departure from sphericity, the larger the percentage of large inter-particle distances. As discussed in section 3.1, the bias dominates when the softening is larger than most inter-particle distances. According to Figure 14 this is expected to happen for larger softening for objects that depart more from sphericity and this is indeed verified in Figure 13.

The second effect that is clear from Figure 13 is that the value of the bias, or, in other words, the values of  $MASE$  on the bias part of the curve, also depends on the departure from sphericity. In particular the larger the departure from sphericity, the smaller this value is. This can again be understood with the discussion in section 3.1. We can simply calculate the value of the bias at infinite softening from equations (6) or (7) by integrating the force of a homogeneous prolate spheroid appropriately over its volume. We find the highest biases for the most spherical objects, and the values decrease as the departure from sphericity increases, in good agreement with the results of Figure 13. Some examples are shown in Figure 15. We see that both oblate and prolate objects have high values of the bias when they are nearly spherical. When they are far from spherical then the bias for the prolate cases is somewhat higher than the bias for the corresponding oblate ones. Figures 13 and 15 show that the effect of shape on the bias can be quite important, changing the corresponding values of  $MASE$  by over an order of magnitude.

Now let us turn to the values of  $MASE$  corresponding to smaller softening. Figure 13 shows that they do not depend much on the shape. This can be understood since, for such values of the softening, it is the noise that affects the error most, and this should not depend on the shape of the object. In particular for values around  $\epsilon_{opt}$  this dependence is negligible. Thus we can conclude that the shape of the homogeneous Ferrers ellipsoid does not influence much either the value of  $\epsilon_{opt}$  which brings the best representation of the forces, or the corresponding value of the error  $MASE_{opt}$ .

## 7 DIFFERENT FORMS OF SOFTENING

In all calculations presented so far we have used the standard Plummer softening, introduced in section 2. There are, however, many alternative ways of introducing the smoothing. For example, instead of using the second power of the softening and of the inter-particle distance in equation

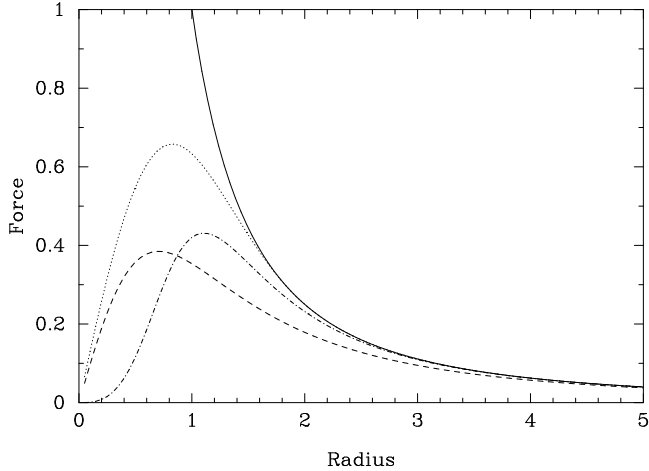


**Figure 16.** Comparison of the forces calculated with three different types of softening to the Newtonian force (solid line). The Plummer softening is given by a dashed line, the power softening with  $p=4$  with a dot-dashed one, and the spline softening with a dotted line.

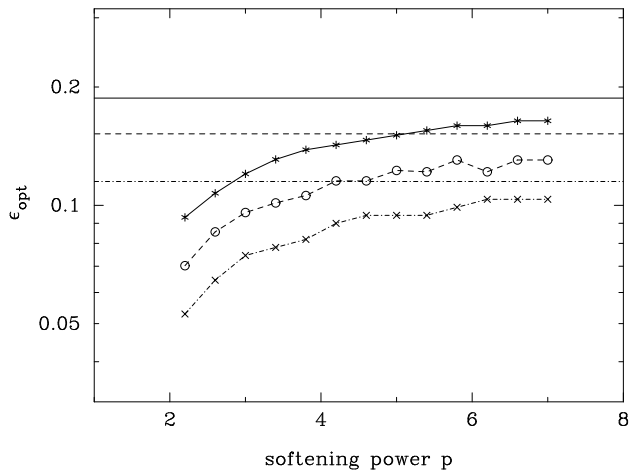


**Figure 17.** Optimal softening as a function of the exponent  $p$  in the power law softening. The solid line and stars correspond to  $N = 10\,000$ , the dashed line and open circles correspond  $N = 30\,000$ , and the dot-dashed line and  $\times$  symbols to  $N = 100\,000$  (cf. text). The corresponding values for the spline softening are given by horizontal lines of the same type.

(1), one could use any other value, including non-integer. Another alternative is to use, instead of the force in a Plummer sphere, the force in a sphere of constant density (e.g. Pfenniger & Friedli 1993, Palouš, Jungwiert & Kopecký 1993), or of any other radial dependence (e.g. Palouš, Jungwiert & Kopecký 1993). Alternatively one could substitute the force between two point masses for the force between two spheres. A few density profiles of the mass within the sphere lend themselves to an easy calculation of the potential

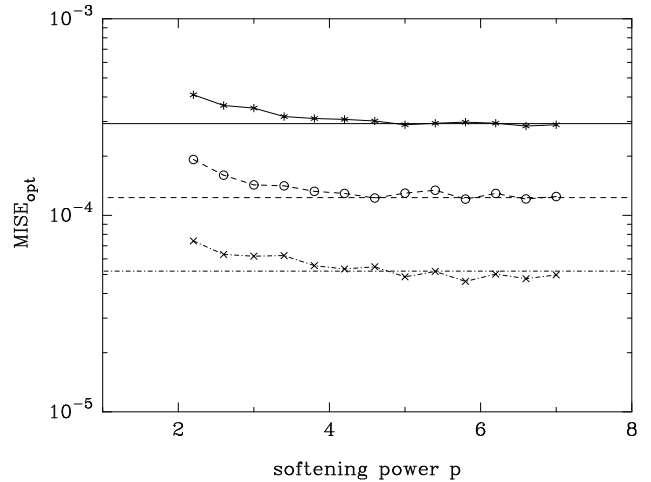


**Figure 18.** As in the previous figure, but for the minimum value of the radial *MISE*.

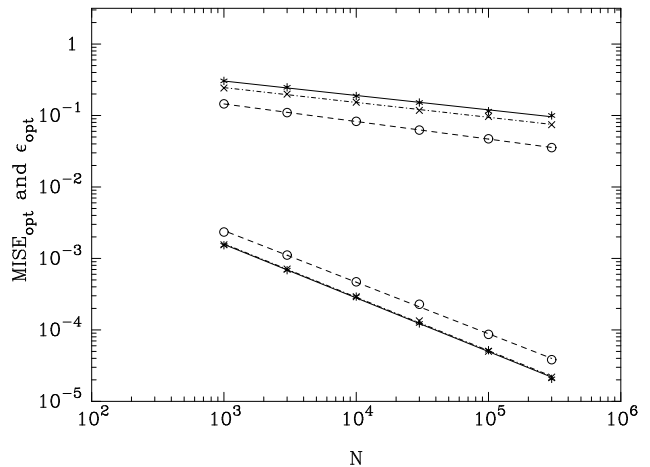


**Figure 19.** Optimal softening and corresponding minimum value of the radial *MISE* as a function of  $N$  for a Plummer sphere. This figure compares the results for a spline softening (solid line), a power softening for  $p = 2$  (dashed line), and a power softening for  $p = 5$  (dot-dashed line).

and corresponding force, in particular certain radial profiles given by polynomials. Such examples have been discussed by Hockney & Eastwood (1981) and by Dyer & Ip (1993).

We will discuss in this section some alternative types of softening and compare how well they fare in the *MISE* test. Since both GRAPE-3 and GRAPE-4 calculate the force only with a Plummer softening, we performed all calculations in this section on workstations, using radial *MISE*, rather than *MASE*, and 64 bit precision. The integration in radial *MISE* was done as described in section 2.

As a first example of an alternative force calculation we will use the spline approximations given by Hernquist & Katz (1989), namely  $\mathbf{F} = -m\mathbf{r}f(r)$ , where

$$f(r) = \begin{cases} 1/\epsilon^3[(4/3) - (6/5)u^2 + (1/2)u^3] & 0 \leq u \leq 1 \\ 1/r^3[-1/15 + (8/3)u^3 - 3u^4 + (6/5)u^5 - (1/6)u^6] & 1 \leq u \leq 2 \\ 1/r^3 & u \geq 2 \end{cases}$$

and  $u = r/\epsilon$ .

Note that for  $r \geq 2\epsilon$  the value of the force in this approximation is exactly the Newtonian force. In other words contrary to the Plummer softening, and to the power-law softening introduced below, the spline softening is approximate only for small distances.

As a second example we will consider an extension of the Plummer softening to values of the exponent other than two. This can be given by

$$\mathbf{F}_i = G \sum_{j=1}^N \frac{m_j(\mathbf{x}_j - \mathbf{x}_i)|\mathbf{x}_i - \mathbf{x}_j|^{p-2}}{(|\mathbf{x}_i - \mathbf{x}_j|^p + \epsilon^p)^{1/p+1}} \quad (11)$$

which for  $p=2$  gives back equation (1). A point to note is that for all values of  $p$ , including the commonly used value  $p = 2$ , these forces tend to the Newtonian one only asymptotically, i.e. even at large distances there is a finite, albeit small, difference between the results they give and those of the Newtonian force. In other words they introduce a small but non-zero smoothing even at large distances, where it isn't necessary.

Figure 16 compares the amplitude of the non-softened Newtonian force with those of the Plummer, the  $p = 4$  power-law and spline softened forces. For this figure we have taken the softening as well as the masses equal to unity. We note that the force that approximates best the Newtonian one is the spline, followed by the higher power softening, while the Plummer softening does the least well of the three. Thus the forces agree better than 5% with the Newtonian one for distances larger than roughly 1.3, 2.2 and 5 softening lengths, correspondingly for the spline,  $p=4$  and Plummer softening.

In order to assess how well each softening can represent the forces in a given mass distribution we calculated radial  $MISE$  values for different values of the softening, for different number of particles in the configuration, and, in the case of the power softening, different values of the exponent  $p$ , roughly in the range from 2 to 8. For all types of softening the  $MISE$  as a function of  $\epsilon$  curves are very similar to those of Figure 1, so we will not repeat them here.

Figure 17 compares the optimal softening ( $\epsilon_{opt}$ ) for the power law softening - as a function of the exponent  $p$  - and for the spline softening. The values were obtained from six hundred realisations of a Plummer sphere of 10 000 particles each, two hundred realisations of 30 000 particles and sixty 100 000 particle realisations. We note that  $\epsilon_{opt}$  increases with  $p$ . Thus comparing  $p = 2.0$  to  $p = 7.0$  we find an increase in  $\epsilon_{opt}$  of roughly a factor of two. The  $\epsilon_{opt}$  value for the spline is somewhat larger than that of the highest  $p$  values. As expected, the optimal softening decreases with increasing number of particles  $N$ . The  $\Delta(\log\epsilon_{opt})$  does not depend notably on the power  $p$ .

Figure 18 compares the minimum value for radial  $MISE$  ( $MISE_{opt}$ ) for the same cases as the previous figure. We note that  $MISE_{opt}$  decreases with  $p$ . Thus comparing  $p = 2.0$  to  $p = 7.0$  we find a decrease in  $MISE_{opt}$  of roughly 30%. The  $MISE_{opt}$  value for the spline is of the order of that of the highest  $p$  values. As expected, the corresponding minimum errors decrease with increasing number of parti-

**Table 3.** Coefficients of the power law fits

Method	A	a	B	b
$p = 2$	0.79	-0.25	0.36	-0.72
$p = 5$	1.05	-0.21	0.28	-0.75
spline	1.22	-0.20	0.28	-0.75

cles  $N$ . The  $\Delta(\log MISE_{opt})$  does not depend notably on the power  $p$ .

Figure 19 compares the optimal softening and the corresponding radial  $MISE$  values as a function of  $N$  for the spline softening and for the power softening for exponents  $p = 2$  and  $p = 5$ . Power laws are satisfactory approximations in all cases, given by

$$\epsilon_{opt} = AN^a$$

and

$$MISE_{opt} = BN^b$$

The values of the coefficients are given in Table 3. The small differences between the coefficients for the Plummer sphere and Plummer softening given here and those given in Table 1 are due to the fact that here we have used radial  $MISE$  while in Table 1  $MASE$ . From this table, as well as from Figure 19, we see that the  $MISE_{opt}$  as a function of  $N$  is more or less the same for the  $p = 5$  and the spline. The  $p = 2$  case gives somewhat bigger values of  $MISE_{opt}$ .

All the above argue that the spline softening as well as the higher values of the power in the power softening give a better representation of the force than the standard Plummer softening. The difference, however, is not as big as one could have inferred from Figure 16, since some of the difference is compensated by an adjustment in  $\epsilon_{opt}$ . Thus Figures 17 and 18 argue for an improvement of 30%, with corresponding changes of  $\epsilon_{opt}$  of a factor of two. This improvement is nevertheless non-negligible, since it would take an increase of the number of particles of roughly 70% to achieve it (cf. section 3.2). The fact that the corresponding value of  $\epsilon_{opt}$  is higher is also an advantage, since, for equally good representations of the forces in the mass distribution, a larger softening allows for large time-steps, and therefore shorter CPU execution times. Last but not least the spline softening necessitates considerably less CPU time per call. This gain in time depends on whether one programs in fortran or C, on what the exponent of the power is, and on the compiler used. We have found ratios roughly between 2 and 10.

## 8 TREECODE

By making some modifications to the standard treecode (Barnes and Hut 1986) it is possible to implement it on a GRAPE system (Makino 1991). In particular the tree should not be descended for each particle separately, but for blocks of particles, as initially proposed by Barnes (1990). Increasing the number of particles in the block makes the interaction list longer and the treecode more accurate. The particular implementation on the Marseille GRAPE systems

is described in A+98, together with some discussion on its performance and accuracy.

We have made calculations of *MASE* using the GRAPE treecode and radial *MISE* with the standard one, for various values of the tolerance and the number of particles  $N$ . The differences between the values corresponding to the same number of particles and different tolerances is rather small. In particular the values obtained with a tolerance of 0.5 or 0.7 are very near those obtained with the direct summation. Only for tolerances larger than 1 do the *MASE* values increase significantly, and even so the differences with the direct summation are always considerably smaller than those obtained by changing the number of particles by factors as those considered e.g. in Figure 1.

## 9 SUMMARY AND DISCUSSION

In this paper we have discussed the value of the softening that allows us to best approximate the true forces within a given mass distribution in an  $N$ -body simulation.

We have first worked with the Plummer sphere and confirmed previous results that, for a given number of particles  $N$ , there is an optimal softening which gives the best approximations to the forces. For smaller values of the softening the noise introduces errors, while for larger there is a systematic bias from the Newtonian force results. We calculated the dependence of the optimal softening on the number of particles  $N$  and confirmed and extended the results of M96 and A+98. We compared the results obtained for integrated and average square errors and found that the latter were considerably less noisy, as could be expected since they involve many more samplings. For this reason *MASE* calculations require considerably more CPU time. Since we have at our disposal two powerful GRAPE systems we performed *MASE* calculations wherever this was possible, i.e. in all cases with direct summation and the standard Plummer softening. We used radial *MISE* calculations for the other softenings. Some of the treecode calculations were done on a GRAPE and some on a workstation. We also find that results obtained with GRAPE-3 agree very well with those obtained on GRAPE-4, despite their differences in accuracy. This is due to the fact that the errors in GRAPE-3 are due to round-off and can thus be considered as random (cf. A+98).

We then worked with other density distributions and found that the density, and the central concentration, have a large influence on the optimal softening and the corresponding error  $MASE_{opt}$ . We first examined the case of two concentric Plummer spheres of different scale-length, and found that the existence of a dense sphere has a large influence on the  $\epsilon_{opt}$  and  $MASE_{opt}$ . We then compared two other density distributions to the Plummer one, namely the homogeneous and the Dehnen sphere. The former is much less centrally concentrated and the latter much more than the Plummer sphere. This confirmed the importance of central concentration on the optimal softening. All our results show that denser configurations necessitate smaller softenings and are never as well represented as less dense ones, i.e. they have considerably larger values of  $MASE_{opt}$ .

Since the choice of the optimal softening depends on the configuration under consideration, and it is rather cumbersome to perform a *MASE* study for every different con-

figuration, we propose a simple way of obtaining a rough estimate of this optimal value. We show that it depends on the mean distance of the nearest neighbours, a quantity which is much easier to calculate or estimate than *MASE*. The precision of this rough estimate should be sufficient in many cases.

We next examined the influence of the shape of the object, with the help of Ferrers ellipsoids of different axial ratios. Although the influence is large on the bias, it is very small for the optimal softening and corresponding  $MASE_{opt}$ .

We then examined two alternative types of softening. One is a power-law softening in which the value of the exponent can have values different than 2, and the other is a spline softening. Large values of the exponent as well as the spline necessitate a larger value of the softening and give a smaller value of the  $MASE_{opt}$ . Since the higher values of the exponent necessitate more CPU time than the spline, it is the latter that provides the best ratio of accuracy to CPU time. The difference, nevertheless, with the standard Plummer softening is not very large.

The treecode results are somewhat less accurate than those obtained with direct summation and the accuracy decreases with increasing tolerance. The differences, however, are small. Thus in order to obtain more accurate results within a given CPU time it should be preferable to increase the number of particles  $N$ , rather than decrease the opening angle. This is particularly true for the standard treecode, where the dependence of the CPU time on the opening angle is stronger (Hernquist 1987, A+98).

The question we have addressed in this paper is obviously of interest for  $N$ -body simulations. If the adopted value of the softening is too small, then the result will be very noisy. In  $N$ -body simulations one considers only one realisation, thus the effect of noise can be very acute. On the other hand if the adopted value of the softening is too large, then the simulation will pertain to another object than was initially desired. In certain cases this may be of little importance, provided the softening is not excessive. This is not, however, always the case. For example if we want to check the stability of a model obtained with the Schwarzschild method (Schwarzschild 1979, 1982), then it is important that the forces approximate as closely as possible those of the model.

The size of structures that need to be analysed has sometimes been used in simulations to set the value of the softening. Our results, however, show that this may not be always possible, and should sometimes be accompanied by a corresponding increase in the number of particles. Indeed if the size of the structures to be analysed are smaller than the  $\epsilon_{opt}$ , then a better resolution can be reached only by increasing the number of particles accordingly.

It is customary in  $N$ -body simulations to use a softening which is constant both in time and position. Our results, however, show that this practice should be questioned.

It is easy to implement a softening which is a function of time. For example in the case we are simulating a collapse the softening at the initial stages can be considerably larger than during the stages of maximum collapse. This could also be said for head-on encounters of galaxies, as e.g. in the formation of ring galaxies, where the central concentration rises considerably over a short period of time. Such a

variation of the softening with time would be easy to implement both on standard software and on GRAPE and could lead to considerably more accuracy.

More challenging is to consider a softening which a function of position, as well as of time, particularly on GRAPE systems. For both GRAPE-3 and GRAPE-4 considerable modifications of the software are necessary. The results of this paper, however, argue that such an effort could be well worth-while. Such a work is in progress (Athanasoula & Lambert, in preparation). It should also be noted that, when changing the softening, corresponding changes in the time step should also be considered.

The fact that the optimal softening is a function of the number of particles used in a simulation affects the CPU time necessary for a given simulation. Suppose that we double the number of particles  $N$  for a given simulation. Then the simulation time will be multiplied by 4 if we are using direct summation and roughly by 2 if we are using a treecode on GRAPE (A+98). However the optimal softening will have also decreased by a factor which for a Plummer type concentration will be of the order of 0.85. This will mean that the time step should also be decreased by a similar factor, and the total CPU time of the simulation increased accordingly. Thus the total CPU time will increase roughly as  $N^{2.24}$  for direct summation and as  $N^{1.24}$  for the treecode.

The dependence of the optimal softening on the number of particles will also affect the relaxation time. Huang, Dubinski & Carlberg (1993) derived the following simple formula for the relaxation time as a function of the softening and the number of particles, assuming that the distribution of particles is homogeneous.

$$T_{relax} = \frac{N}{8 \ln(R/\epsilon)} T_{cross} \quad (12)$$

In the above  $T_{cross}$  is the crossing time and  $R$  is some characteristic radius of the system. Replacing the softening by its optimal value, which is a function of the number of particles, we find that the relaxation time will grow somewhat less rapidly than expected if the softening was not a function of  $N$ .

These are the prices to pay for a simulation with better resolution, with reduced particle noise and with more accurately calculated forces.

**Acknowledgments.** We would like to thank Yoko Funato, Dave Merritt, Christos Vozikis and Mattias Wahde for useful discussions. We would also like to thank the IGRAP, the INSU/CNRS and the University of Aix-Marseille I for funds to develop the GRAPE computing facilities used for the calculations in this paper.

## References.

Aarseth S. J. 1963 MNRAS, 126, 223  
 Athanasoula E. 1993, in Problèmes à N corps et dynamique Gravitationnelle, eds. F. Combes et E. Athanasoula, Editions de l'Observatoire de Paris  
 Athanasoula E., Bosma A., Lambert J. C., Makino J, 1998, MNRAS, 293, 369 (A+98)  
 Barnes J., 1990, J. Comput. Phys., 87, 161  
 Barnes J. and Hut P. 1986, Nat, 324, 446

Barnes J. and Hut P. 1989, ApJS, 70, 389  
 Binney J. and Tremaine S. D. 1987, Galactic Dynamics, Princeton University Press, Princeton  
 Dehnen W. 1993, MNRAS, 265, 250  
 Dyer C. C., Ip P. S. S. 1993 ApJ, 409, 60  
 Ferrers N.M. 1877, Q. J. Pure Appl. Math., 14, 1  
 Hernquist L.: 1987, ApJS, 64, 715  
 Hernquist L., Hut P. and Makino J. 1993, ApJ, 402, L85  
 Hernquist L., Katz N., 1989 ApJS, 70, 419  
 Hockney R.W., Eastwood J.W.: 1981, "Computing simulations using particles", McGraw-Hill, New York  
 Huang S., Dubinski J., Carlberg R.G. 1993, ApJ, 404, 73  
 Kawai A., Fukushige T., Taiji M., Makino J., Sugimoto D. 1997, PASJ, 49, 607  
 Kawai A., Makino J. 1999 Proceedings of the Ninth SIAM Conference on Parallel Processing for Scientific Computing, SIAM  
 Makino J. 1991, PASJ, 43, 621  
 Makino J. 1994, in V.G. Gurzadyan, D. Pfenniger, eds, Ergodic Concepts in Stellar Dynamics, Springer Verlag, p. 131  
 Makino J. Taiji M. 1998, Scientific Simulations with special-purpose computers, John Wiley, Chichester  
 Makino, J., Taiji, M., Ebisuzaki, T., Sugimoto, D. 1997, ApJ, 480, 432  
 Merritt D. 1996, AJ, 111, 2462  
 Palous J., Jungwiert B., Kopecký J. 1993, A&A, 274, 189  
 Pfenniger D. Friedli D. 1993 A&A, 270, 561  
 Press W.H., Flannery B.P., Teukolsky S.A., Vetterling W.T. 1988 Numerical Recipes in C, Cambridge Univ. press.  
 Salmon J.J., Warren, M.S.: 1994 J. Comp. Phys., 11, 136  
 Schwarzschild M. 1979, ApJ, 232, 236  
 Schwarzschild M. 1982, ApJ, 263, 599  
 Sellwood J.A.: 1987, ARA&A, 25, 151  
 Teuben P.J 1995 - in R. Shaw, H.E. Payne and J.J.E. Hayes, eds, Astronomical Data Analysis Software and Systems IV, ASP conference series 77, p. 398